J. Fluid Mech. (1997), *vol.* 336, *pp.* 331–350

The propagation of premixed flames in closed tubes

By MOSHE MATALON[1] AND PHILIPPE METZENER[2]

[1]Department of Engineering Sciences and Applied Mathematics, Northwestern University, Evanston, IL 60208-3125, USA

[2]Département de Mathématique, Ecole Polytechnique Fédérale de Lausanne, Lausanne, CH-1015, Switzerland

(Received 4 April 1996 and in revised form 19 November 1996)

A nonlinear evolution equation that describes the propagation of a premixed flame in a closed tube has been derived from the general conservation equations. What distinguishes it from other similar equations is a memory term whose origin is in the vorticity production at the flame front. The two important parameters in this equation are the tube's aspect ratio and the Markstein parameter. A linear stability analysis indicates that when the Markstein parameter α is above a critical value α_c the planar flame is the stable equilibrium solution. For α below α_c the planar flame is no longer stable and there is a band of growing modes. Numerical solutions of the full nonlinear equation confirm this conclusion. Starting with random initial conditions the results indicate that, after a short transient, a flat flame develops when $\alpha > \alpha_c$ and it remains flat until it reaches the end of the tube. When $\alpha < \alpha_c$, on the other hand, stable curved flames may develop down the tube. Depending on the initial conditions the flame assumes either a cellular structure, characterized by a finite number of cells convex towards the unburned gas, or a tulip shape characterized by a sharp indentation at the centre of the tube pointing toward the burned gases. In particular, if the initial conditions are chosen so as to simulate the elongated finger-like flame that evolves from an ignition source, a tulip flame evolves downstream. In accord with experimental observations the tulip shape forms only after the flame has travelled a certain distance down the tube, it does not form in short tubes and its formation depends on the mixture composition. While the initial deformation of the flame front is a direct result of the hydrodynamic instability, the actual formation of the tulip flame results from the vortical motion created in the burned gas which is a consequence of the vorticity produced at the flame front.

1. Introduction

Studies of premixed flames in closed tubes are of fundamental interest for the insight they provide into the burning process and into the interaction between the flame and the underlying flow field. They have also significant technological relevance: flame propagation in closed vessels has direct application to internal combustion engine processes and it represents the initial and transition stages in the development of a detonation wave.

Although in the absence of the gravitational force a planar flame front is always a possible solution of the conservation equations, it is seldom observed in experiments. The hydrodynamic instability (Darrieus 1938; Landau 1944) does not permit the

existence of flames that are too flat and stable curved fronts are generated instead. Premixed flames propagating in open tubes are generally convex toward the unburned gas (Uberoi 1959). It has been argued (Zel'dovich *et al.* 1980) that this configuration is much more stable than planar fronts. Experimental observations of flames propagating in closed tubes, on the other hand, reveal interesting and unexpected features. Following ignition the flame grows from a hemisphere surrounding the ignition source to a nearly flat shape extending over the cross-section of the tube. It then undergoes an inversion: the leading edge of the flame becomes near the walls and the flame trails behind at the centre of the tube forming a cusp that points toward the burned gases. This flame shape is referred to as a *tulip flame* in the literature. A tulip flame also forms in a tube closed at the ignition end and open at the other end.

An extensive study of the tulip flame phenomenon that includes photographs of the inversion process was first reported by Ellis (1928). This work and the subsequent studies by Guénoche (1964) revealed that a tulip flame forms only after the flame has travelled a certain distance down the tube and that it does not form in short tubes (of aspect ratio less than two). It was also found that the formation of the tulip flame depends on the composition of the combustible mixture and on the initial pressure in the tube. Another interesting observation reported by Guénoche is that in very long tubes, i.e. of aspect ratio ~ 20, the inversion of the flame front can reverse itself. The centre part of the tulip flame, which is pointing toward the burned gas, starts accelerating and overtakes the outer edges. The flame shape is now again convex towards the unburned gases. This process repeats itself a number of times with the flame undergoing a series of inversions until it reaches the end of the tube. Finally it should be pointed out that there have been some recent experiments (Starke & Roth 1986; Dunn-Rankine, Barr & Sawyer 1986; Clanet & Searby 1996) on this phenomenon which have provided more detailed information on the flow and pressure fields in the tube.

There have been also a number of numerical simulations (Rotman & Oppenheim 1986; N'konga *et al.* 1992; Gonzalez, Borghi & Saouab 1992) aimed at reproducing the tulip flame and possibly clarifying the physical mechanisms responsible for its formation. Based on these studies, and on the experimental work referred to earlier, various possible explanations have been suggested. These include: the cooling of the burned gas which would cause expansion of the fresh mixture (Ellis 1928), the interaction between the flame and pressure waves (Guénoche 1964), viscous drag at the walls (Lewis & von Elbe 1987), large circulation induced in the unburned gas (Dunn-Rankine *et al.* 1986; Rotman & Oppenheim 1986) and the Darrieus–Landau instability (Gonzales *at al.* 1992; N'konga *at al.* 1992). However, the actual cause of the formation of tulip flames has not been conclusively determined. A more fundamental approach has been recently undertaken by Matalon & McGreevy (1994) who examined the stability of planar flame fronts propagating in closed tubes. The linear analysis presented in that paper identifies conditions for the onset of an instability which are in general agreement with the experimental records. However, as a result of the linearization invoked, the analysis does not uniquely determine the shape of the flame that develops beyond the instability threshold and therefore does not completely describe the inversion process leading to the tulip flame.

The mathematical model adopted in the present study is similar to that used by Matalon & McGreevy (1994). The flame is treated as a surface of density discontinuity in an otherwise inviscid isentropic flow. The flame is characterized by its temperature and by the rate at which it consumes the reactants, namely the burning rate. The flame temperature determines the density jump across the discontinuity while the burning

rate determines the propagation speed or, equivalently, the shape and location of the discontinuity. For curved flames the resulting free boundary problem must, in general, be solved numerically. A simplification is obtained if one treats the dimensionless heat release q as a perturbation parameter. This approximation enables one to explicitly determine the flow field on either side of the flame so that the problem reduces to a single nonlinear integro-differential equation for the position of the flame front. This equation, when expressed in terms of the distortion $\varphi(y,t)$ from a flat flame, was first presented in Matalon (1995). It takes the form

$$\frac{1}{q}\frac{\partial\varphi}{\partial t} = \alpha\frac{\partial^2\varphi}{\partial y^2} + \frac{1}{2}\left(\frac{\partial\varphi}{\partial y}\right)^2 - \frac{1}{L}\varphi + \mathscr{J}(\varphi) \tag{1.1}$$

where L is the tube's aspect ratio (length/width), α is the Markstein parameter and the exact form of the linear integral operator $\mathscr{J}(\cdot)$ is given below in equation (4.8). An important element of (1.1) is the memory effect contained in $\mathscr{J}(\varphi)$. This effect has its origin in the vorticity production at the flame front which turns out to be an essential ingredient for properly describing the inversion that characterizes the formation of tulip flames. Although the limit of small heat release does not fully characterize combustion processes, it is nevertheless one that was found extremely useful in a variety of theoretical studies (see for example Buckmaster & Ludford 1982). It appears, in this case as well, that this approximation retains the essential physics of the problem as is evident from the numerical results of (1.1) which are in complete qualitative agreement with experimental observations.

When the Markstein parameter α exceeds a critical value $\alpha_c \approx 0.05L$, the planar front is absolutely stable. For $0 < \alpha < \alpha_c$, there is a range of wavenumbers for which, in the finite time available, small disturbances superimposed on a flat flame eventually grow to a magnitude much larger than their initial size. Disturbances of longer wavelength are unable to grow to a significant size while those of shorter wavelength are stabilized by diffusion. Nonlinear effects limit the growth and stable curved flames, that propagate at a nearly constant speed, develop down the tube. The flame assumes either a cellular shape, characterized by a finite number of cells convex toward the unburned gas, or a tulip shape whose characteristics were described above. The new structure is very sensitive to the initial data. In particular, when starting with initial conditions that simulate the elongated finger-like flame that evolves from an ignition point source, a tulip flame results. The initial deformation of the flame front is a direct consequence of the hydrodynamic instability as is evident from the linear stability analysis of (1.1) discussed in §5; see also the more general linear analysis of Matalon & McGreevy (1994). The following events leading to the tulip flame are a consequence of nonlinearities. The curved flame generates vorticity which, due to the confinement, is accumulated in the burned gas behind the flame front. The vortical motion thus created, and the sense of the circulation in the flow field, depend strongly on the initial conditions. From the elongated finger-like flame, a pair of vortices is created in the burned gas with a circulation that tends to advect the centre part of the flame upstream, thus creating the peculiar shape referred to as a the tulip flame.

The evolution equation (1.1) can be simplified when the tube is infinite in extent, that is when the flame is propagating in a tube open at both ends. In this limit the term $\mathscr{J}(\varphi)$ simplifies significantly and one recovers the integro-differential equation derived by Sivashinsky (1977) for freely propagating flames. Sivashinsky's equation contains no memory effect and is apparently unable to describe the inversion phenomenon that

characterizes tulip flames. It was argued (Dold & Joulin 1995) that the equation that results by adding a second-order time derivative to Sivashinsky's equation is capable of describing the inversion phenomenon associated with tulip flames. This new equation was obtained by synthesizing Sivashinsky's equation with the linear dispersion relation of Darrieus and Landau which describes the growth of disturbances resulting from the hydrodynamic instability. Our equation (1.1), which has been derived from first principles, shows that for long but finite tubes the reminiscent of the memory effects include the second-order time derivative that they have suggested. There are, however, additional terms of the same order of magnitude that must also be retained in the equation, for consistency.

The paper is organized as follows. In §2 the governing equations and the model treating the flame as a surface of discontinuity are presented. Planar flames are described in §3. The derivation of the evolution equation is given in §4, followed by a linear stability analysis of planar fronts in §5 and numerical results of the full nonlinear equation in §6. Simplifications of the evolution equation for long tubes are discussed in §7.

2. Governing equations

A premixed combustible mixture of density ρ_0, temperature T_0 and pressure p_0 occupies the volume of a closed tube. The mixture consists of a deficient reactant with an initial mass fraction Y_0 and a molecular weight W. When ignited, at the left end of the tube say, a flame propagates towards its right end. The present discussion is concerned with the post-ignition events. It is therefore assumed that at time $t = 0$ a flame has already been established at the left end of the tube, and our objective is to determine its evolution for $t > 0$. The flow is assumed to be inviscid; that is the boundary layers that develop in the unburned gas as a result of the flame propagation remain thin and have no effect on the flame shape. The combustion mixture is considered an ideal gas with constant material properties. Finally, the combustion process is assumed to occur under adiabatic conditions.

The governing equations, expressing conservation of the mixture's mass, momentum and energy and a mass balance for the deficient reactant are given by

$$\frac{\mathrm{D}\rho}{\mathrm{D}t} + \rho\nabla\cdot\boldsymbol{v} = 0, \tag{2.1a}$$

$$\rho\frac{\mathrm{D}\boldsymbol{v}}{\mathrm{D}t} = -\nabla p, \tag{2.1b}$$

$$\rho c_p\frac{\mathrm{D}T}{\mathrm{D}t} - \nabla\cdot\lambda\nabla T = \frac{\mathrm{D}p}{\mathrm{D}t} + Q\mathscr{B}\left(\frac{\rho Y}{W}\right)\mathrm{e}^{-E/R^oT}, \tag{2.1c}$$

$$\rho\frac{\mathrm{D}Y}{\mathrm{D}t} - \nabla\cdot\rho\mathscr{D}\nabla Y = -\mathscr{B}\left(\frac{\rho Y}{W}\right)\mathrm{e}^{-E/R^oT}, \tag{2.1d}$$

where $\boldsymbol{v}, p, \rho, Y$ and T are the velocity, pressure, density, mass fraction and temperature respectively, and $\mathrm{D}/\mathrm{D}t \equiv \partial/\partial t + \boldsymbol{v}\cdot\nabla$ is the convective derivative. The specific heats of the mixture, c_p and c_v, are assumed constant and so is their ratio $\gamma = c_p/c_v$. The thermal conductivity λ and the molecular diffusivity associated with the deficient reactant in the mixture $\mathscr{D}$ are, in general, temperature dependent. The chemical activity has been modelled by a one-step, irreversible, overall chemical reaction of Arrhenius type with an activation energy E and a pre-exponential factor $\mathscr{B}$. The

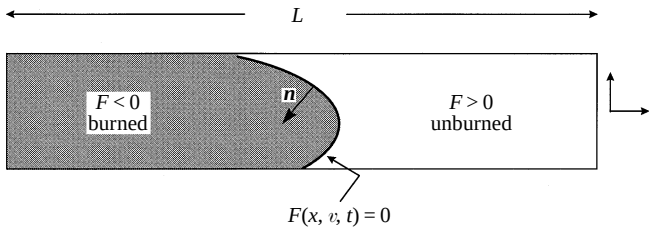

FIGURE 1. Schematic of a flame propagating in a tube.

total heat of combustion is denoted by Q and the universal gas constant by R^o. The equation of state takes the form

$$p = \rho R^o T / \bar{W} \tag{2.2}$$

with $\bar{W}$ an average molecular weight. Finally, the boundary conditions along the walls of the tube are

$$\hat{\boldsymbol{n}} \cdot \boldsymbol{v} = \hat{\boldsymbol{n}} \cdot \nabla T = \hat{\boldsymbol{n}} \cdot \nabla Y = 0 \tag{2.3}$$

where $\hat{\boldsymbol{n}}$ is a unit vector normal to the walls.

Based on the following observations the governing equations (2.1*a*)–(2.1*d*) can be significantly simplified (for more details, see Matalon 1995).

(i) The laminar flame speed, $v_0 \sim$ 50–100 cm s^{-1}, is much smaller then the speed of sound. Hence the representative Mach number $\mathscr{M} \equiv v_0/(\gamma p_0/\rho_0)^{1/2} \ll 1$. Acoustic disturbances therefore propagate relatively fast and the pressure is almost instantaneously equalized throughout the tube. The pressure can therefore be expressed as

$$p(\boldsymbol{x}, t) = P(t) + \gamma \mathscr{M}^2 p'(\boldsymbol{x}, t) + \cdots$$

where $P(t)$ represents the mean pressure level and p' accounts for the small spatial variations. Note that the small pressure gradients, $\mathscr{M}^2 \nabla p'$, are needed to balance the small momentum changes in equation (2.1*b*).

(ii) The diffusion length $\ell_d = \lambda_o/\rho_0 c_p v_0 \sim 10^{-2}$ cm, is typically much smaller than a characteristic dimension of the tube, for example the width of the tube ℓ. Hence the parameter $\ell_d/\ell \ll 1$. The $O(\ell_d/\ell)$ diffusion and reaction terms in (2.1*c*), (2.1*d*) are therefore negligibly small except in the thin flame zone separating the burned from the unburned gases. Viewed on the length scale ℓ the thin flame may be treated as a surface of density discontinuity which propagates according to some rule that is determined from the analysis of its internal structure.

We thus obtain, after some manipulations,

$$\nabla \cdot \boldsymbol{v} = -\frac{1}{\gamma P} \frac{\mathrm{d}P}{\mathrm{d}t}, \tag{2.4a}$$

$$\rho \frac{\mathrm{D}\boldsymbol{v}}{\mathrm{D}t} = -\nabla p', \tag{2.4b}$$

$$\frac{\mathrm{D}}{\mathrm{D}t}\left(\rho^{-1} P^{1/\gamma}\right) = 0, \tag{2.4c}$$

$$\rho T = P. \tag{2.4d}$$

In writing these equations we have introduced dimensionless variables as follows. The width of the tube, ℓ, has been used as a unit for length, the laminar flame speed, v_0,

as a unit for the velocity, ℓ/v_0 as a unit for time and the initial state of the fresh mixture T_0, p_0, ρ_0, Y_0 as units for the temperature, pressure, density and reactant mass fraction, respectively.

If the flame front is described by $F(\boldsymbol{x}, t) = 0$, with $\boldsymbol{n} = -\nabla F/|\nabla F|$ a unit normal pointing toward the burned gas (see figure 1), the Rankine–Hugoniot jump relations across the flame are

$$[\rho(\boldsymbol{v}\cdot\boldsymbol{n} - V_f)] = 0, \tag{2.5a}$$

$$[p' + \rho(\boldsymbol{v}\cdot\boldsymbol{n} - V_f)(\boldsymbol{v}\cdot\boldsymbol{n})] = 0, \tag{2.5b}$$

$$[\boldsymbol{v}\times\boldsymbol{n}] = 0, \tag{2.5c}$$

$$[T] = q. \tag{2.5d}$$

Here $V_f = |\nabla F|^{-1}(\partial F/\partial t)$ is the normal velocity of the front, $q = QY_0/c_pT_0$ is the heat release parameter and $[\cdot]$ denotes the jump in the quantity defined as its value in the burned side minus that in the unburned side.

Equation (2.4c) implies that the entropy $\sim \ln\mathscr{E} \equiv \ln(\rho^{-1}P^{1/\gamma})$ is conserved along particle paths. Since the state of the fresh mixture is initially uniform, the entropy of the unburned gas remains constant at all times. Consequently, the temperature and density remain uniform throughout the unburned gas region and rise in time according to the law of adiabatic compression; hence

$$T = P^{(\gamma-1)/\gamma}, \quad \rho = P^{1/\gamma} \qquad \text{for } F(\boldsymbol{x}, t) > 0. \tag{2.6}$$

By applying the jump relationship (2.5d), the flame temperature can be determined as

$$T_f = T_a + P^{(\gamma-1)/\gamma} - 1 \tag{2.7}$$

where $T_a = 1+q$ is the adiabatic flame temperature, i.e. the temperature of a premixed flame propagating freely under isobaric conditions. The entropy of the burned gas at the flame front is therefore

$$\mathscr{E}_f = 1 + qP^{-(\gamma-1)/\gamma}. \tag{2.8}$$

Note that the flame temperature is continuously increasing as the pressure builds up in the tube. On the other hand $\mathscr{E}_f$ decreases in time. Hence the gas elements that burn first have a larger entropy which implies that the highest temperature in the tube is not necessarily reached at the flame front but rather in the neighbourhood of the ignition point. Consequently temperature (or entropy) gradients develop in the burned gas region; for more details see Matalon (1995).

In the burned gas region one finds from (2.4c), (2.4d) that

$$T = P^{(\gamma-1)/\gamma}\,\mathscr{E}(\boldsymbol{x}, t), \quad \rho = P^{1/\gamma}/\mathscr{E}(\boldsymbol{x}, t) \qquad \text{for } F(\boldsymbol{x}, t) < 0 \tag{2.9}$$

where the entropy function $\mathscr{E}$ is determined by solving $\mathrm{D}\mathscr{E}/\mathrm{D}t = 0$ subject to $\mathscr{E} = \mathscr{E}_f$ at the flame front. To complete the system one needs equations for $P(t)$ and $F(\boldsymbol{x}, t)$; these depend on the internal structure of the flame and will be discussed next.

It is more convenient to write an expression for the mass burning rate,

$$M \equiv \rho(\boldsymbol{v}\cdot\boldsymbol{n} - V_f)|_{\text{flame}},$$

instead of an equation for the flame position $F(\boldsymbol{x}, t)$. For a premixed flame propagating in free space, the analysis of the flame structure (Matalon & Matkowsky 1982) yields

$$M = 1 - \alpha q\,\{V_f\nabla\cdot\boldsymbol{n} - \boldsymbol{n}\cdot\nabla\times(\boldsymbol{v}\times\boldsymbol{n})\} \tag{2.10}$$

where $\alpha = O(\ell_d/\ell)$ is the Markstein parameter and the expression in the curly brackets

constitutes the flame stretch (Matalon 1983). Hence the burning rate depends on the curvature of the flame front and on non-uniformities in the incoming flow field. This expression has been derived for unconfined flames and will be adopted here. We note that the Markstein parameter α depends on the mixture composition through the Lewis number $Le = \lambda_0/\rho_0 c_p \mathscr{D}_0$ (the ratio of the thermal to molecular diffusivities). For a planar flame front (2.10) reduces to $M = 1$ (i.e. $\rho_0 v_0$ in dimensional form). Although as a result of pressure buildup the burning velocity v_0 of a planar flame may also increase in time (McGreevy & Matalon 1992), we have neglected these variations in the present discussion.

An equation for the mean pressure P can be obtained by combining (2.1*a*) and (2.1*c*) and integrating the resulting equation throughout the volume of the tube. One finds

$$\frac{\mathrm{d}P}{\mathrm{d}t} = \frac{\gamma q}{L} \int_{\mathscr{A}_f} M \, \mathrm{d}\mathscr{A}_f \tag{2.11}$$

where $\mathscr{A}_f$ is the flame surface area and L is the dimensionless tube's length (or the tube's aspect ratio). If the reactants are totally consumed during the process, the final pressure P_e is obtained independent of the flame dynamics and is a property of the given mixture. Forming the enthalpy equation by adding (2.1*c*) to (2.1*d*) after multiplying the latter by q, then integrating this equation throughout the volume of the tube, one finds that $P_e = 1 + \gamma q$. The pressure level in the vessel is determined by solving (2.11) subject to $P = 1$ at $t = 0$. The condition $P = P_e$ then serves to determine the total time that it takes for the flame to reach the end of the tube.

3. Planar flames

Let the flame front be described by $x = x_f(t)$, the axial velocity $\boldsymbol{v} = u\boldsymbol{i}$ is given by

$$u = \begin{cases} -(\dot{P}/\gamma P)x & \text{for} \quad 0 < x < x_f \\ (\dot{P}/\gamma P)(L - x) & \text{for} \quad x_f < x < L \end{cases}$$

indicating that the fresh mixture is compressed towards the far right end of the tube while the burned gas moves away toward the ignition end. The dot over P represents differentiation with respect to time. From (2.5*a*) one finds that

$$x_f(t) = L\left(1 - \frac{P_e - P}{P_e - 1} P^{-1/\gamma}\right)$$

where the pressure level increases linearly according to

$$P = 1 + \gamma q t/L. \tag{3.1}$$

This also implies that the total time for the flame to travel from one end of the tube to the other is L. The entropy function in the burned gas is given by $\mathscr{E} = \psi(xP^{1/\gamma})$ where the function $\psi(\eta)$ is determined implicitly from the relations

$$\psi(\eta) = 1 + qP^{-(\gamma-1)/\gamma},$$
$$\eta = x_f P^{1/\gamma}.$$

Note that ψ is a decreasing function that takes the value $1 + q$ at zero and reaches $1 + qP_e^{-(\gamma-1)/\gamma}$ as the independent variable approaches $LP_e^{1/\gamma}$. Finally, the pressure deviations from the mean, $p'(x, t)$, can be calculated from (2.4*b*) and (2.5*b*).

For future reference we note that these results can be simplified for small q as follows. The axial velocity and the pressure field are respectively given by

$$u \sim \begin{cases} -qx/L + \gamma q^2 xt/L^2 + \cdots & \text{for} \quad x < x_f \\ q(1-x/L) - \gamma q^2(1-x/L)(t/L) + \cdots & \text{for} \quad x > x_f, \end{cases}$$

$$p' \sim \begin{cases} -q - q^2(\gamma+1)(x^2/2L^2) + \cdots & \text{for} \quad x < x_f \\ -q^2\{(\gamma+1)(x/2L-1)(x/L) + (1+2\gamma)(t/L)\}\cdots & \text{for} \quad x > x_f, \end{cases}$$

with the flame position expressed as

$$x_f \sim t\left\{1 + q(1-t/L) - \tfrac{1}{2}q^2(\gamma+1)(1-t/L)t/L + \cdots\right\}.$$

The function $\psi(\eta)$ has the explicit form

$$\psi(\eta) \sim 1 + q - q^2(\gamma-1)\eta/L + \cdots$$

so that the density and temperature are given by

$$\rho \sim \begin{cases} 1 - q(1-t/L) + q^2\left\{1 - t/L + (\gamma-1)x/L - (\gamma-1)(t^2/2L^2) + \cdots\right\} & \text{for} \quad x < x_f \\ 1 + qt/L - q^2(\gamma-1)(t^2/2L^2) + \cdots & \text{for} \quad x > x_f, \end{cases}$$

$$T \sim \begin{cases} 1 + q\{1 + (\gamma-1)t/L\} + q^2(\gamma-1)\left\{(t-x)/L - t^2/2L^2\right\} + \cdots & \text{for} \quad x < x_f \\ 1 + q(\gamma-1)t/L - q^2(\gamma-1)(t^2/2L^2) + \cdots & \text{for} \quad x > x_f. \end{cases}$$

Note that these expansions, despite being valid for small q, exhibit all the essential characteristics of the exact solution.

4. The evolution equation

The mathematical problem describing non-planar flames is indeed formidable. It consists of a coupled system of time-dependent nonlinear partial differential equations further complicated by the existence of a free moving boundary. In this form it is only amenable to numerical simulations. An alternative approach is to consider an asymptotic limit and derive a single equation that describes the evolution of the flame front. The limit considered here is $q \ll 1$. Although this limit does not fully characterize combustion processes it is nevertheless one that was found extremely useful in a variety of theoretical studies, as discussed in the introduction.

Restricting attention to a two-dimensional flow, we introduce the following expansions:

$$\left.\begin{aligned} u &= \bar{u}(x,t) + q^2 U(x,y,t) + \cdots, \\ v &= \qquad\quad q^2 V(x,y,t) + \cdots, \\ p' &= \bar{p}'(x,t) + q^2 \Pi(x,y,t) + \cdots, \end{aligned}\right\} \tag{4.1}$$

with the flame front position expressed in the form

$$x = \bar{x}_f(t) + q\varphi(y,t) + \cdots$$

Here, the overbar denotes the planar solution described in § 3. Upon substituting in equation (2.11) one finds that the mean pressure may be expressed as

$$P = 1 + \gamma qt/L + O(q^3).$$

The governing equations (2.4*a*)–(2.4*b*) reduce to

$$\frac{\partial U}{\partial x} + \frac{\partial V}{\partial y} = 0, \tag{4.2a}$$

$$\frac{\partial U}{\partial t} = -\frac{\partial \Pi}{\partial x}, \qquad \frac{\partial V}{\partial t} = -\frac{\partial \Pi}{\partial y}, \tag{4.2b}$$

and the jump relations (2.5*a*)–(2.5*c*), when expressed at the mean flame position $x = t$, simplify to

$$[U] = [\Pi] = 0, \quad [V] = \frac{\partial \varphi}{\partial y}. \tag{4.3}$$

A curved flame front is therefore equivalent to a flat vortex sheet whose non-uniform strength is given by the last condition in (4.3). The equation for the burning rate (2.10) becomes

$$\frac{\partial \varphi}{\partial t} = q\left\{\alpha \frac{\partial^2 \varphi}{\partial y^2} + \frac{1}{2}\left(\frac{\partial \varphi}{\partial y}\right)^2 - \frac{1}{L}\varphi + U^*\right\} \tag{4.4}$$

where $U^* = U(x = t, y, t)$. Note that in the present approximation the most significant contribution to flame stretch is the flame front curvature; flow non-uniformities have a secondary effect on the propagation velocity. The small parameter q is retained in equation (4.4) because secondary effects appear to be of physical significance and because the complete combustion process evolves over various time scales. Rather than rescaling time repeatedly, it is preferable for numerical computation to keep the equation in this form and use a relatively small q for consistency. The boundary and initial conditions will be discussed in due course.

It is useful to introduce the vorticity vector which, following (4.1), is expanded as

$$\nabla \times \boldsymbol{v} = q^2 \varpi \, \boldsymbol{k} + \cdots.$$

According to Helmholtz theorem the flow in the unburned gas is irrotational, so that $\varpi = 0$ for $t < x < L$. The same conclusion cannot be drawn for the flow in the burned gas because vorticity is produced at the curved flame front. Since equations (4.2*b*) imply that $\partial \varpi / \partial t = 0$, one concludes that $\varpi = \varpi(x, y)$ for $0 < x < t$. We note parenthetically that there is another source of vorticity which results from the spatial non-uniformities in the density and pressure fields in the burned gas region. This gives rise to a non-zero baroclinic vector (Matalon 1995) which is negligibly small within the present approximation.

The system of equations (4.2*a*),(4.2*b*) can be solved using a Fourier transform in y. If $\widetilde{f}(x, k, t)$ denotes the Fourier transform of the function $f(x, y, t)$ one finds, after satisfying the jump relationships (4.3) and the boundary conditions $U = 0$ at $x = 0$ and L,

$$\widetilde{U} = \begin{cases} k\, B(k,t)\, \sinh kx + k^2 \displaystyle\int_0^x \cosh[k(x-\xi)]\, \widetilde{\varphi}(k,\xi)\, \mathrm{d}\xi & \text{for} \quad x < t \\ -k\, C(k,t)\, \sinh[k(L-x)] & \text{for} \quad x > t, \end{cases}$$

$$\widetilde{V} = \mathrm{i}k \begin{cases} B(k,t)\, \cosh kx + \widetilde{\varphi}(k,x) + k \displaystyle\int_0^x \sinh[k(x-\xi)]\, \widetilde{\varphi}(k,\xi)\, \mathrm{d}\xi & \text{for} \quad x < t \\ C(k,t) \cosh[k(L-x)] & \text{for} \quad x > t, \end{cases}$$

where

$$B(k,t) = -k \int_0^t \frac{\cosh[k(L-\tau)]}{\sinh kL}\, \widetilde{\varphi}(k,\tau)\, \mathrm{d}\tau,$$

$$C(k,t) = -k \int_0^t \frac{\cosh k\tau}{\sinh kL}\, \widetilde{\varphi}(k,\tau)\, \mathrm{d}\tau.$$

Consequently

$$\widetilde{\varpi} = \begin{cases} \mathrm{i}k(\partial\widetilde{\varphi}/\partial t)|_{t=x} & \text{for} \quad 0 < x < t \\ 0 & \text{for} \quad t < x < L. \end{cases} \tag{4.5}$$

Thus, at the flame front,

$$\widetilde{U}^*(k,t) = \frac{k^2 \sinh[k(L-t)]}{\sinh kL} \int_0^t \cosh k\tau\, \widetilde{\varphi}(k,\tau)\, \mathrm{d}\tau. \tag{4.6}$$

Equation (4.4) now yields the evolution equation

$$\frac{1}{q}\frac{\partial\varphi}{\partial t} = \alpha\frac{\partial^2\varphi}{\partial y^2} + \frac{1}{2}\left(\frac{\partial\varphi}{\partial y}\right)^2 - \frac{1}{L}\varphi + \mathscr{J}(\varphi), \tag{4.7}$$

where the linear operator $\mathscr{J}$ is defined such that

$$\mathscr{J}(\varphi) = \frac{1}{2\pi}\int_{-\infty}^{\infty}\int_{-\infty}^{\infty}\left[\int_0^t G(k,t;\tau)\,\varphi(\eta,\tau)\,\mathrm{d}\tau\right] \mathrm{e}^{\mathrm{i}k(y-\eta)}\,\mathrm{d}k\,\mathrm{d}\eta \tag{4.8}$$

with the kernel $G(k,t;\tau)$ given by

$$G(k,t;\tau) = \frac{k^2 \sinh[k(L-t)]\,\cosh k\tau}{\sinh kL}.$$

This equation must be supplemented with boundary conditions along the side walls of the tube and an initial shape at $t = 0$. The discussion of the boundary conditions will be postponed until needed.

An important aspect of the evolution equation (4.7) is the *memory* effect contained in $\mathscr{J}(\varphi)$. To understand its physical significance we integrate (4.8) by parts with respect to t and find that $\mathscr{J}(\varphi) = \mathscr{J}_1(\varphi)$ - $\mathscr{J}_2(\varphi)$ where

$$\mathscr{J}_1(\varphi) = \frac{1}{2\pi}\int_{-\infty}^{\infty}\int_{-\infty}^{\infty}\frac{k\,\sinh[k(L-t)]}{\sinh kL}\sinh kt\;\varphi(\eta,t)\,\mathrm{e}^{\mathrm{i}k(y-\eta)}\,\mathrm{d}k\,\mathrm{d}\eta \tag{4.9a}$$

$$\mathscr{J}_2(\varphi) = \frac{1}{2\pi}\int_{-\infty}^{\infty}\int_{-\infty}^{\infty}\frac{k\,\sinh[k(L-t)]}{\sinh kL}\left[\int_0^t \sinh k\tau\,\frac{\partial\varphi}{\partial\tau}\mathrm{d}\tau\right]\mathrm{e}^{\mathrm{i}k(y-\eta)}\,\mathrm{d}k\,\mathrm{d}\eta. \tag{4.9b}$$

These two terms correspond to the potential and rotational contributions to the flow field, respectively. In particular, the memory term in $\mathscr{J}_2(\varphi)$ represents the accumulated effect of the vorticity production at the flame (see (4.5)). There have been theoretical studies that assume a potential flow throughout the combustion field. Our result demonstrates that this *ad hoc* approach may exclude important dynamical behaviours. For example, unlike equation (4.7), a potential flow model is unable to describe the flame inversion observed during the development of a tulip flame. Finally, we point out that for infinitely long tubes, equation (4.7) reduces to that derived by Sivashinsky (1977) for freely propagating flames, as discussed in §7.

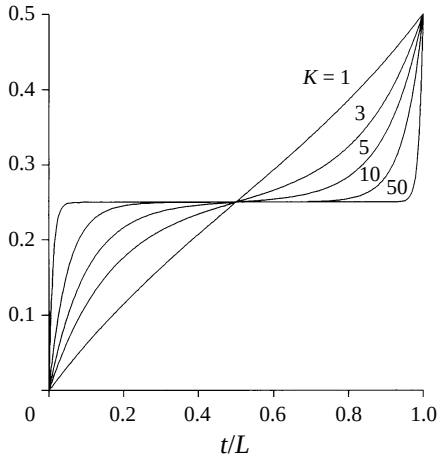

FIGURE 2. The dependence of the second term in the expression for A_1 versus t/L, for several values of the wavenumber K.

5. Linear analysis

Consider small disturbances superimposed to the planar flame front, $\varphi = 0$, of the form $\varphi = A(t)\mathrm{e}^{\mathrm{i}ky}$ with k the wavenumber. After linearization equation (4.7) reduces to

$$\frac{\mathrm{d}A}{\mathrm{d}t} + q\left(\frac{1}{L} + \alpha k^2\right) A = \frac{qk^2 \sinh[k(L-t)]}{\sinh(kL)} \int_0^t \cosh(k\tau)\, A(\tau)\, \mathrm{d}\tau.$$

We now seek an expansion of the form

$$A = A_0 + qA_1 + q^2 A_2 + \cdots$$

where A_0 is a constant determined by the initial condition. Consequently

$$\frac{1}{A_0}\frac{\mathrm{d}A_1}{\mathrm{d}t} = -\left(\frac{1}{L} + \alpha k^2\right) + \frac{k \sinh[k(L-t)] \sinh kt}{\sinh kL}$$

which, when solved subject to $A_1(0) = 0$, yields

$$A_1 = A_0 \left\{ \left(\frac{k}{2}\coth kL - \frac{1}{L} - \alpha k^2\right) t - \frac{1}{4}\left(1 + \frac{\sinh[k(2t-L)]}{\sinh kL}\right)\right\}. \tag{5.1}$$

We observe that when $\alpha < 0$, there are always values of k for which $\dot{A}_1(0) > 0$; the planar flame in this case is considered unstable. But when $\alpha > 0$ we find that $\dot{A}_1(0) < 0$ for all k, so that initially disturbances of all wavelengths are damped. An instability may be associated with the development that follows thereafter if A_1 changes sign. In the following, a mode of wavenumber k will be considered *unstable* if for some $0 < t < L$ the amplitude $A_1(t)$ becomes positive. The time for the onset of instability, $t = t^*$ say, is obtained by setting $A_1(t^*) = 0$.

In figure 2 the second term on the right-hand side of (5.1) is plotted as a function of t/L for several values of $K = kL$. Since the first term varies linearly with t/L, a necessary condition for instability is that the slope $m = (K/2)\coth K - 1 - (\alpha/L)K^2$ of this line exceeds $1/4$. This implies that for instability α/L must be sufficiently small. Since as K increases $\coth K$ approaches 1 rapidly, $m(K) \simeq K/2 - 1 - \alpha K^2/L$, and the

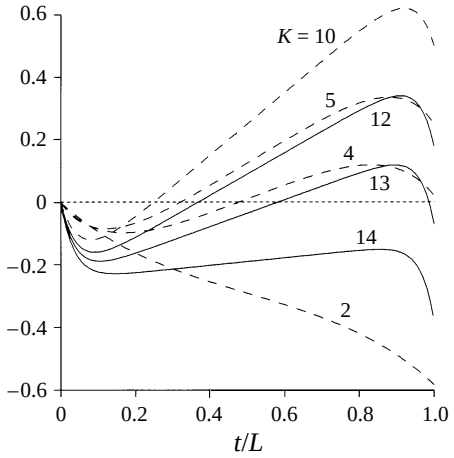

FIGURE 3. The amplitude A_1 as a function of time, t/L, for several values of the wavenumber K; calculated for $\alpha = 0.046$.

necessary condition for instability is approximately

$$\frac{\alpha}{L} < 0.05. \tag{5.2}$$

The unstable modes are then restricted to

$$\frac{1}{4\alpha}\left[1-(1-20\alpha/L)^{1/2}\right] \;<\; k \;<\; \frac{1}{4\alpha}\left[1+(1-20\alpha/L)^{1/2}\right]. \tag{5.3}$$

These approximate expressions are found to be reasonably good when compared to the exact conditions calculated numerically. Finally we point out that the lower bound on k should be further limited by the width of the tube.

It is well known that the density decrease across the flame front gives rise to a hydrodynamic instability (Darrieus 1938; Landau 1944). In closed tubes the limitation imposed by the finite width of the tube and by the finite duration of the process does not allow the long-wave disturbances to develop significantly. The growing modes are therefore limited to disturbances of wavenumber $k > k_{min}$. Diffusional thermal effects, on the other hand, play an important role primarily on the short-wavelength disturbances. Depending on the Markstein parameter α, or more specifically on the Lewis number associated with the deficient reactant in the mixture, diffusional–thermal effects have either stabilizing or destabilizing influences. For $\alpha < 0$ they are destabilizing so that all disturbances with $k > k_{min}$ grow; for $\alpha > 0$ they are stabilizing so that the growing modes are restricted to those with wavenumber $k_{min} < k < k_{max}$. There is therefore a range of unstable modes when $\alpha > 0$, given by (5.3), which disappears as $\alpha \to 0.05L$.

In figure 3 we have plotted the amplitude A_1 as a function of time for a range of wavenumbers and for $\alpha = 0.046\,L$. We observe that the short- as well as the long-wavelength disturbances are damped. Instabilities are confined to moderate wavelength disturbances, or more precisely disturbances with wavenumber k approximately in the range $2.64 < kL < 8.22$. These results are in qualitative agreement with the linear theory of Matalon & McGreevy (1994) which was based on the complete hydrodynamical model, i.e. without recourse to the assumption of small q.

6. Numerical simulations – finite length tubes

For prescribed initial conditions, $\varphi(y,0) = \varphi^0(y)$, the evolution equation (4.7) must be solved for $0 < t \leqslant L$ in the domain $0 \leqslant x \leqslant L$, $-1 \leqslant y \leqslant 1$. We require the solution to be symmetric with respect to $y = 0$ and to satisfy the requirement $\partial\varphi/\partial y = 0$ along the walls of the tube. The last requirement is a direct consequence of the no-penetration condition $V = 0$, and is consistent with the assumption of thermally insulating walls. The problem has been solved numerically using a spectral method.

An appropriate representation of the solution that satisfies the required conditions is

$$\varphi(y,t) = \sum_{n=0}^{N} \tilde{\varphi}(k,t) \cos ky$$

with $k = n\pi$. In the Fourier (k,t)-space, equation (4.7) can be rewritten in the form

$$\tilde{\theta}_t = -k \tanh kt \; \tilde{\theta} + \tilde{\varphi}, \tag{6.1a}$$

$$\tilde{\varphi}_t = q \left\{ \tfrac{1}{2} k^2 g(k,t) \; \tilde{\theta} - (1/L + \alpha k^2)\tilde{\varphi} + \tfrac{1}{2} \widetilde{(\varphi_y^2)} \right\}, \tag{6.1b}$$

where

$$\tilde{\theta}(k,t) = \frac{1}{\cosh kt} \int_0^t \tilde{\varphi}(k,\tau) \cosh k\tau \, \mathrm{d}\tau$$

and the kernel $g(k,t)$ is given by

$$g(k,t) = 1 + \frac{\mathrm{e}^{-2kt} - \mathrm{e}^{-2k(L-t)}}{1 - \mathrm{e}^{-2kL}}.$$

The initial conditions for this system are

$$\tilde{\varphi}(k,0) = \widetilde{\varphi^o}(k), \qquad \tilde{\theta}(k,0) = 0. \tag{6.2}$$

For a given N the system of ordinary differential equations (6.1*a*), (6.1*b*) has been integrated with the help of the NAG routine D02EBF which uses a variable-order, variable-step method and implements a backward differentiation formula. The number N has been fixed following the empirical rule that $N = 4k_{max}$, where k_{max} is the upper bound of the interval (5.3) that identifies the range of the unstable modes. The quadratic term $\widetilde{(\varphi_y^2)}$ has been computed using a fast Fourier transform algorithm for the cosine transforms; it has been evaluated with $2N$ collocations points which is found to lead to an arithmetically exact computation.

The results are shown in figures 4–9, where snapshots of the flame shape are shown at constant time intervals. Except where otherwise indicated, the heat release parameter has been chosen as $q = 0.5$ and the length of the tube was taken as $L = 10$. As indicated in the captions an amplification factor has often been used in order to improve visualization.

6.1. *Diffusional–thermal effects*

The Markstein parameter α is the only mixture-sensitive parameter in our model. As noted earlier α depends on the Lewis number and hence on the mixture's composition. Starting with random but identical initial conditions the three figures 4 (*a*)–(*c*) illustrate the development of the flame front for three different values of α. For $\alpha = 0.15$, the planar flame front is stable according to the linear theory; see equation (5.2).

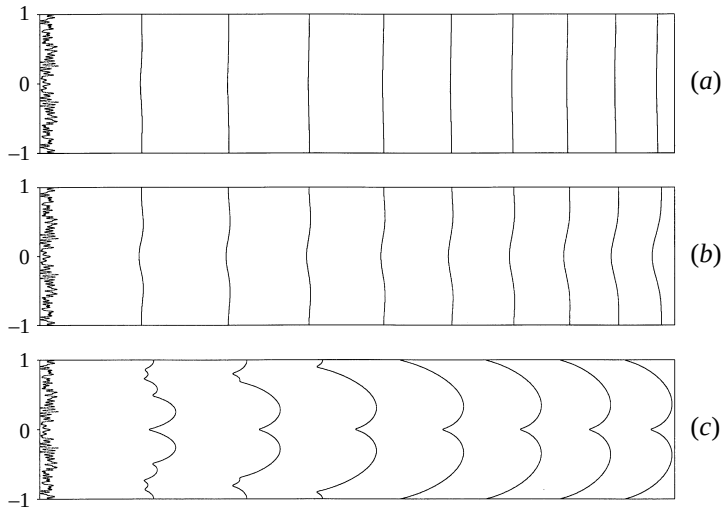

FIGURE 4. The development of the flame front from random initial conditions, for (*a*) $\alpha = 0.15$; (*b*) $\alpha = 0.08$; (*c*) $\alpha = 0.01$. The distortions from a flat flame have been enhanced by a factor of 5 to improve visualization.

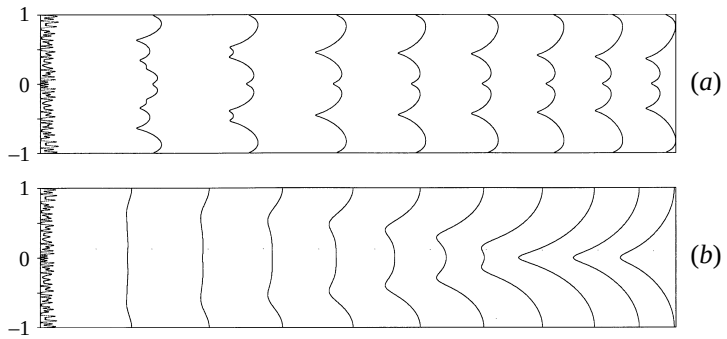

FIGURE 5. The development of the flame front from random initial conditions, different from those used in figure 4; for (*a*) $\alpha = 0.01$; (*b*) $\alpha = 0.04$. The distortions from a flat flame have been enhanced by a factor of 5 to improve visualization.

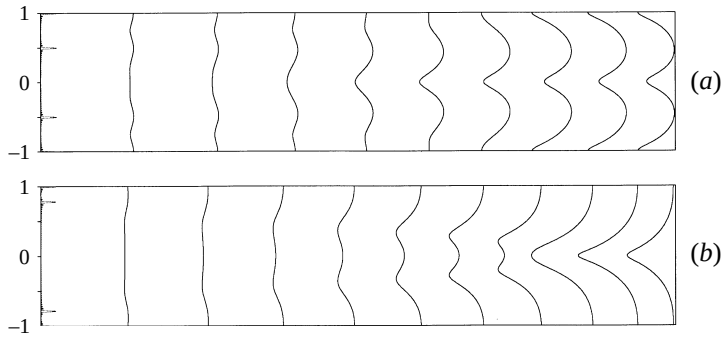

FIGURE 6. The development of the flame front from initial conditions corresponding to a pair of pulses located at (*a*) $y = \pm 1/2$; (*b*) $y = \pm 3/4$. In both cases $\alpha = 0.04$. The distortions from a flat flame have been enhanced by a factor of 5.

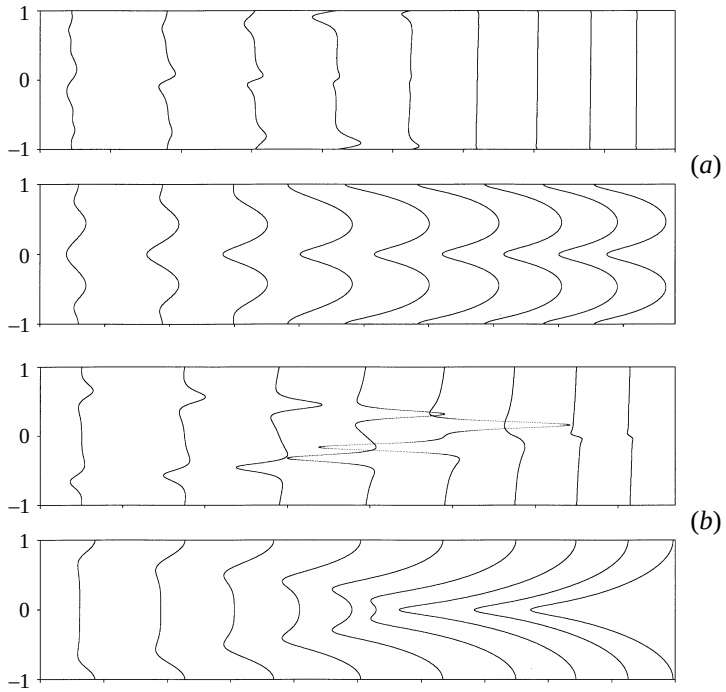

FIGURE 7. The vorticity distribution along the sheet $x = t$ during the development of (*a*) a cellular flame; (*b*) a tulip flame. Calculated with $\alpha = 0.04$. The distortions from a flat flame here have been enhanced by a factor of 10.

Figure 4 (*a*) confirms this result; after an initial transient the flame flattens out and a nearly planar front propagates towards the end of the tube. For a value $\alpha = 0.08$ near the instability threshold the flame beyond the initial transient does not flatten out; it remains slightly curved until it reaches the end of the tube (see figure 4*b*). The pattern that evolves once the planar front becomes unstable depends of course on the number of excited modes. We recall that according to the linear theory these are restricted to wavenumbers in the range (5.3). Figure 4 (*c*), plotted for $\alpha = 0.01$, shows that the small cells that develop during the initial phase of propagation disappear and a two-cell structure emerges towards the end of the tube. This structure seems to be the near-equilibrium solution, as is evident from the fact that the flame retains its shape during the last phase of propagation and propagates at a nearly constant speed.

6.2. *Initial conditions*

The development of the flame depends strongly on the initial data. Figure 5 (*a*) shows the development of the flame for the same value of α as used in figure 4 (*c*), but with different random initial conditions. One finds that the flame remains in a transient state until it reaches the end of the tube. The small cells are continuously shrinking while the large cells are increasing in size. A two-cell structure might have developed if the tube were longer. Figure 5 (*b*) shows that for a somewhat larger value of α, $\alpha = 0.04$, and with the same initial conditions as used in figure 5 (*a*) a tulip flame emerges towards the end of the tube. We were unable to reproduce the tulip shape with the initial data of figure 4.

To further examine the sensitivity to the initial conditions we have chosen an initial disturbance that corresponds to a pair of pulses located symmetrically with respect to axis of the tube, but at different positions with respect to the walls. In figure 6 (*a*), for example, the pulses are located halfway between the centreline and the walls, i.e. at $y = \pm 1/2$; in figure 6(*b*) the pulses are located closer to the walls, or specifically at $y = \pm 3/4$. In the former, the equilibrium state appears to be a two-cell structure while in the latter it is a tulip flame.

6.3. *Vorticity production*

The development of the flame beyond the initial transient has been redrawn in figure 7 along with the vorticity distribution at the unperturbed position of the flame, i.e. at $x = t$, for the same parameters and initial conditions as those used in figure 6. Here, an amplification factor of 10 has been used.

As pointed out earlier the curved flame is equivalent to a flat vortex sheet of non-uniform strength located at $x = t$. According to (4.5), the strength of the vortex sheet is given by

$$\varpi = \left.\frac{\partial^2 \varphi}{\partial t \partial y}\right|_{t=x}.$$

The non-uniform distribution of vorticity along the sheet induces a velocity field which, according to the Biot–Savart law, tends to advect the flame in the axial direction in one or the other direction. In the first case, shown in figure 7 (*a*), two pairs of vortices are created, one on each side of the centreline. The sense of the circulation, shown in the figure, is such that the flame is advected upstream near the walls and along the centerline. The relatively stronger circulation near the walls is responsible for the cellular pattern that develops towards the end of the tube. The nearly uniform vorticity distribution at the end of the tube is additional evidence that the flame has nearly reached an equilibrium state. In the second case, shown in figure 7 (*b*), only one pair of vortices is formed. The sense of circulation is such as to advect the flame into a shape whereby its centre part becomes increasingly more convex with respect to the burned gases. The larger magnitude of the vorticity is responsible for the sharp indentation observed at the centre of the tube in contrast with that seen in figure 7 (*a*).

6.4. *Tulip flames*

As described in the introduction, experimental observations reveal that flames propagating in closed tubes often acquires a tulip shape. In a typical experiment, the combustible mixture is ignited at a point at one end of the tube. During the first phase of the burning a spherical flame, centred around the ignition point, propagates outward. It then gradually develops into a hemisphere that continues to grow into an elongated finger. Once the flame makes contact with the walls, it flattens out and a tulip shape develops thereafter. In order to simulate the experimental conditions we consider, as initial condition, an elongated finger-like flame shape. The results are shown in figure 8. In the short tube, $L = 5$, the flame flattens out and remains flat until it reaches the end of the tube. In a moderate tube, $L = 10$, the flame first flattens out but as it propagates downstream its centre part becomes increasingly more convex toward the burned gases. In a yet longer tube, $L = 20$, the tulip flame clearly forms before the mixture burns completely. The elongated finger-like flame is clearly responsible for the magnitude and sense of circulation which, as pointed out earlier, induces a flow field that forces the formation of the tulip flame. Our results

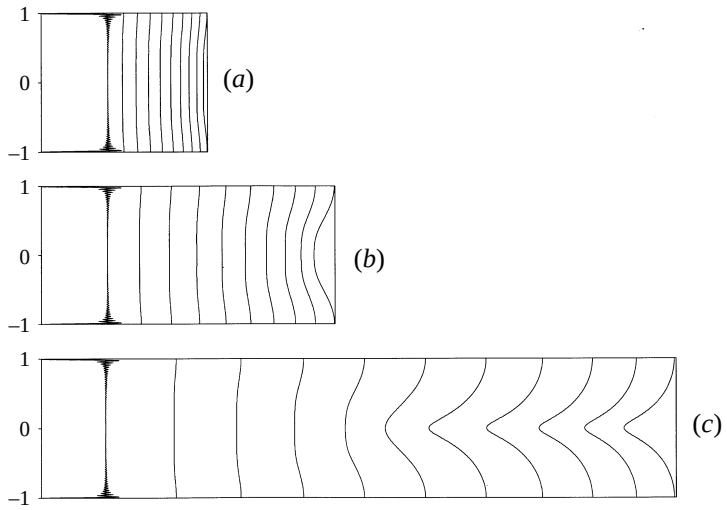

FIGURE 8. The development of a tulip flame in tubes of length (*a*) $L = 5$, (*b*) $L = 10$, (*c*) $L = 20$; calculated for $\alpha = 0.06$. The distortions from a flat flame have been enhanced by a factor of 5.

are in agreement with experimental records which indicate that, when a tulip flame emerges, it forms only after the flame has travelled half of the length of the tube and that it does not form in short tubes.

6.5. *Heat release*

In figure 9 we illustrate the dependence of the flame development towards a tulip shape on the heat release parameter q. No amplification factor has been used in this case so that the figure shows the actual size of the flame. The snapshots are presented at intervals of one unit of time so that the relative propagation velocity could be easily detected by observation. The flame remains nearly planar when q is small, and its propagation speed is much slower than the propagation of the tulip flame. Thus, an increase in the heat release causes enhancement in the motion of the distorted flame. Consequently the total propagation time is shortened. Since, as pointed out earlier, the final pressure P_e is independent of the flame dynamics, there will be a sharp increase in pressure during the last stages of propagation. A boundary layer analysis is thus required to properly describe the events occurring when the flame nears the end of the tube.

7. Long tubes

For very long tubes, $L \to \infty$, the kernel $g(k,t) \sim 1$, and the system (6.1*a*), (6.1*b*) simplifies to

$$q\widetilde{\theta}_s = -|k|\widetilde{\theta} + \widetilde{\varphi}, \tag{7.1a}$$

$$\widetilde{\varphi}_s = \tfrac{1}{2}k^2\,\widetilde{\theta} - \alpha k^2\widetilde{\varphi} + \tfrac{1}{2}\widetilde{(\varphi_y^2)}, \tag{7.1b}$$

in terms of the slow time $s = qt$.

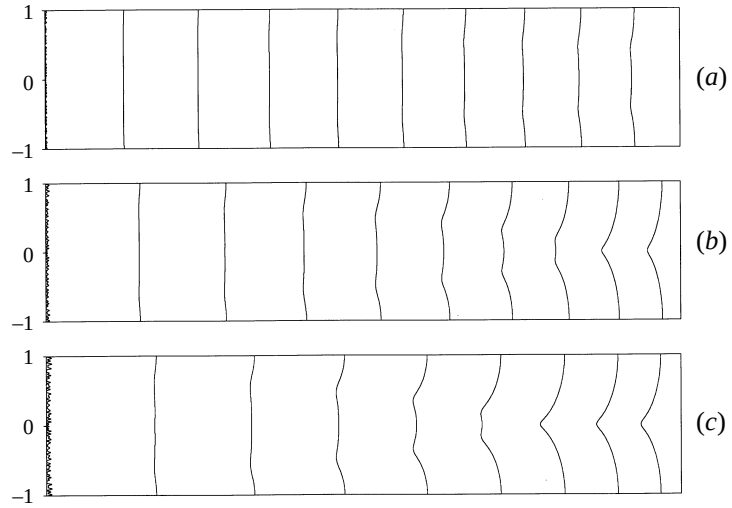

FIGURE 9. The dependence of the flame development on the heat release parameter (*a*) $q = 0.25$, (*b*) $q = 0.5$, (*c*) $q = 0.75$; calculated for $\alpha = 0.04$. The figure displays the actual distortion of the flame; no amplification factor has been used.

All memory effects are now confined to $s \approx 0$. Ignoring these effects yields $|k|\widetilde{\theta} = \widetilde{\varphi}$ which, when substituted into (7.1*b*), gives

$$\widetilde{\varphi}_s = \tfrac{1}{2}|k|\,\widetilde{\varphi} - \alpha k^2 \widetilde{\varphi} + \tfrac{1}{2}\widetilde{(\varphi_y^2)}.$$

The first term on the right-hand side is the Darrieus–Landau growth rate (the hydrodynamic instability). The second term is the influence of diffusion which is stabilizing or destabilizing depending on whether α is positive or negative, respectively. In real space, one obtains the evolution equation

$$\varphi_s = \alpha\varphi_{yy} + \tfrac{1}{2}\varphi_y^2 + \tfrac{1}{2}\mathscr{I}(\varphi) \tag{7.2}$$

with $\mathscr{I}$ given by

$$\mathscr{I}(\varphi) = \frac{1}{2\pi}\int_{-\infty}^{\infty}\int_{-\infty}^{\infty} |k|\ \varphi(\eta, s)\,\mathrm{e}^{\mathrm{i}k(y-\eta)}\,\mathrm{d}k\,\mathrm{d}\eta.$$

This equation has been previously derived by Sivashinsky (1977) for freely propagating flames. If memory effects are now retained, one finds from (7.1*a*) that

$$\widetilde{\theta} = \left[\widetilde{\theta}(0) + \frac{1}{q}\int_0^s \mathrm{e}^{|k|\sigma/q}\widetilde{\varphi}(k,\sigma)\mathrm{d}\sigma\right]\mathrm{e}^{-s|k|/q}. \tag{7.3}$$

Substituting into (7.1*b*) after differentiating the latter with repect to s yields

$$q(\varphi_s - \alpha\varphi_{yy} - \tfrac{1}{2}\varphi_y^2)_s + \mathscr{I}(\varphi_s - \alpha\varphi_{yy} - \tfrac{1}{2}\varphi_y^2 - \tfrac{1}{2}\mathscr{I}(\varphi)) = 0. \tag{7.4}$$

Equation (7.2) has been used successfully to describe the wrinkling and the formation of cusps that are often observed on large-scale freely propagating flame fronts and are a manifestation of the hydrodynamic instability (Michelson & Sivashinsky, 1977). This equation, however, seems unable to describe the inversion of tulip flames. As a remedy Dold & Joulin (1995) wrote down an equation similar to (7.4) but with the first bracket containing only the term φ_{ss}. This was obtained by synthesizing Sivashinsky's equation (7.2) with the linear dispersion relation of Darrieus (1938) and

Landau (1944). Our derivation shows that two other terms, φ_{yys} and $(\varphi_y^2)_s$ are of equal magnitude and should not be neglected in a self-consistent treatment. The origin of the nonlinear term in this equation is in the normal velocity of the front V_f. Within the present approximation it is easy to verify that

$$V_f \sim q(\bar{x}_f)_s + q^2(\varphi_s - \tfrac{1}{2}\varphi_y^2)$$

so that both the time derivative and the nonlinear terms are of the same magnitude. When differentiated with respect to time, they will retain the same magnitude so that both are expected to appear together on the left-hand side of equation (7.4). Numerical solutions of (7.4) that illucidate the peculiar dynamics of premixed flames in very long tubes will be reported in a future study.

One of the authors (M.M) gratefully acknowledges the support of the National Science Foundation and of the microgravity combustion program under NASA sponsorship.

REFERENCES

Buckmaster, J. D. & Ludford, G. S. S. 1982 *Theory of Laminar Flames*. Cambridge University Press.

Clanet, C. & Searby, G. 1996 On the tulip flame phenomenon. *Combust. Flame* **105**, 225.

Darrieus, G. 1938 Propagation d'un front de flamme. Unpublished manuscript; presented at Le Congrés de Mecanique Appliquée.

Dold, J. W. & Joulin, G. 1995 An evolution equation modeling inversion of tulip flames. *Combust. Flame* **100**, 450.

Dunn-Rankin, D., Barr, P. K. & Sawyer, R. F. 1986 Numerical and experimental study of tulip flame formation in a closed vessel. *Twenty-First Symp. (Intl) on Combustion*, p. 1291. The Combustion Institute.

Ellis, O. C. de C. 1928 Flame movement in gaseous explosive mixtures. *Fuel in Science and Practice* **7**, 502.

Gonzalez, M., Borghi, B. & Saouab, A. 1992 Interaction of a flame front with its self-generated flow in an enclosure: the tulip flame phenomenon. *Combust. Flame* **88**, 201.

Guénoche, H. 1964 Flame propagation in tubes and in closed vessels. In *Nonsteady Flame Propagation* (ed. G. H. Markstein). Macmillan.

Landau, L. D. 1944 On the theory of slow combustion. *Acta Physicochimica URSS* **19**, 77.

Lewis, B. & Elbe, G. von 1987 *Combustion, Flames and Explosions in Gases*, third edition. Academic.

Markstein, G. H. 1964 Theory of flame propagation. In *Nonsteady Flame Propagation*. (ed. G. H. Markstein). Macmillan.

Matalon, M. 1983 On flame stretch. *Combust. Sci. Tech.* **31**, 169.

Matalon, M. 1995 Flame propagation in closed vessels. *Mathematical Modeling in Combustion Science* (ed. J. Buckmaster & T. Takeno), vol. 124, p. 239. Springer.

Matalon, M. & Matkowsky, B. J. 1982 Flames as gasdynamics discontinuities. *J. Fluid Mech.* **124**, 239.

Matalon, M. & McGreevy J. L. 1994 The initial development of a tulip flame. *Twenty-Fifth Symp. (Intl) on Combustion*, p. 1407. The Combustion Institute.

McGreevy, J. L. & Matalon, M. 1992 Lewis number effects on the propagation of premixed flames in closed tubes. *Combust. Flame* **91**, 213.

Michelson, D. M. & Sivashinsky, G. I. 1977 Nonlinear analysis of hydrodynamic instability in laminar flames - II. Numerical experiments. *Acta Astronautica* **4**, 1207.

N'konga, B., Fernandez, G., Guillard, H. & Larrouturou, B. 1992 Numerical investigations of the tulip flame instability - comparisons with experimental results. *Combust Sci. Tech.* **87**, 69.

Rotman, D. A. & Oppenheim, A. K. 1986 Aerothermic properties of stretched flames in enclosures. *Twenty-First Symp. (Intl) on Combustion*, p. 1303. The Combustion Institute.

Sivashinsky, G. I. 1977 Nonlinear analysis of hydrodynamic instability in laminar flames - I. Derivation of the basic equations. *Acta Astronautica* **4**, 1177.

Starke, R. & Roth, P. 1986 An experimental investigation of flame behavior during cylindrical vessel explosion. *Combust. Flame* **66**, 249.

Uberoi, M. S. 1959 Flow field of a flame in a channel. *Phys. Fluids* **2**, 72.

Williams, F. A. 1965 *Combustion Theory*, 2nd Edn. Benjamin/Cummings.

Zel'Dovich, A. G., Istratov, A. G., Kidin N. I. & Librovich V. B. 1980 Flame propagation in tubes: hydrodynamics and stability. *Combust. Sci. Tech.* **24** 1.